Dalton Transactions

RSC Publishing

PAPER

View Article Online
View Journal | View Issue

Cite this: *Dalton Trans.*, 2013, **42**, 6523

Luminescent $GdVO_4:Eu^{3+}$ functionalized mesoporous silica nanoparticles for magnetic resonance imaging and drug delivery

Shanshan Huang,[a,b] Ziyong Cheng,[a] Ping'an Ma,[a] Xiaojiao Kang,[a,b] Yunlu Dai[a,b] and Jun Lin*[a]

Received 31st December 2012,
Accepted 13th February 2013

DOI: 10.1039/c3dt33114h

www.rsc.org/dalton

Luminescent $GdVO_4:Eu^{3+}$ nanophosphor functionalized mesoporous silica nanoparticles (MSN) were prepared (denoted as $GdVO_4:Eu^{3+}$@MSN). The *in vitro* cytotoxicity tests show that the sample has good biocompatibility, which indicates that the nanocomposite could be a promising candidate for drug delivery. Flow cytometry and confocal laser scanning microscopy (CLSM) confirm that the sample can be effectively taken up by SKOV3 ovarian cancer cells and A549 lung adenocarcinoma cells. It was also shown that the $GdVO_4:Eu^{3+}$@MSN brightened the T_1-weighted images and enhanced the r_1 relaxivity of water protons, which suggested that they could act as T_1 contrast agents for magnetic resonance (MR) imaging. It was found that the carriers present a pH-dependent drug release behavior for doxorubicin (DOX). The composites show a red emission under UV irradiation due to the $GdVO_4:Eu^{3+}$ nanophosphors. Furthermore, the PL intensity of the composite shows correlation with the cumulative release of DOX. These results suggest that the composite can potentially act as a multifunctional drug carrier system with luminescent tagging, MR imaging and pH-controlled release property for DOX.

Introduction

Mesoporous silica materials have been widely used as supports for drug delivery, because of their large surface area, large pore volume, chemically modifiable surfaces and biocompatibility.[1–8] Moreover, the highly ordered mesoporous structure of the mesoporous silica material makes it an excellent candidate for accommodating guest molecules, providing a cavity that can protect the loaded drugs from degradation and denaturization.[9–18] The pH responsive drug release systems based on the mesoporous silica nanoparticles have been explored to target the acidic environment of cancerous tissue, as the pH in tumor and inflammatory tissues is more acidic than in blood and normal tissue, with endosomes and lysosomes exhibiting even lower pH values.[19,20] Capping agents, such as functional groups,[21–23] polymers,[24,25] polyelectrolytes,[26–30] ring-shaped compounds,[31–34] and inorganic particles[35,36] have been introduced on the surface of mesoporous silica nanoparticles to control the release of guest molecules at various pH values. Host–guest interactions (electrostatic,[37,38] covalent bonding[39] and coordination bonding[40–42]) have been utilized to achieve the pH-responsive goal.

$GdVO_4:Eu^{3+}$ phosphors are excellent red-emitting materials that can be applied in many fields, such as cathode ray tubes, lamps and X-ray detectors.[43] Gd^{3+} is commonly used as a positive contrast agent for magnetic resonance imaging (MRI) in current clinical applications.[44–48] The use of ultrafine europium-doped gadolinium vanadate ($Gd_{1-x}Eu_xVO_4$, $x = 0.35$) nanophosphors as biological labels for *in vitro* bioimaging as well as MRI contrast applications has been explored.[49] Gd^{3+} incorporated mesoporous Gd_2O_3@MCM-41 has been reported as an efficient MRI contrast agent.[50] $Gd_2O_3:Eu^{3+}$ functionalized hydrogel modified luminescent rattle-type mesoporous silica microspheres can act as a spin–lattice relaxation time (T_1)-MR contrast agent.[51] Multifunctional PAA-modified upconversion luminescent $GdVO_4:Ln^{3+}$ (Ln = Yb/Er, Yb/Ho, Yb/Tm) hollow nanospheres have been successfully prepared.[52] However, to the best of our knowledge, the study of the $GdVO_4:Eu^{3+}$ functionalized mesoporous silica nanoparticles as MRI contrast agents and drug delivery systems have not been reported so far.

In this article, luminescent $GdVO_4:Eu^{3+}$ functionalized mesoporous silica nanoparticles with diameters in the range of 80–120 nm were synthesized. The *in vitro* MTT assay shows that the as-prepared sample has good biocompatibility, which indicates that the composite could be a promising candidate

[a]*State Key Laboratory of Rare Earth Resource Utilization, Changchun Institute of Applied Chemistry, Chinese Academy of Sciences, Changchun 130022, PR China*
[b]*University of Chinese Academy of Sciences, Beijing 100049, PR China.*
E-mail: jlin@ciac.jl.cn;; Fax: +86-431-85698041; Tel: +86-431-85262031

for drug delivery. Cell uptake of the composite was examined by flow cytometry and confocal laser scanning microscopy. Because of the Gd^{3+} ions in the composites, the $GdVO_4$:Eu^{3+}@MSN can act as a spin–lattice relaxation time (T_1)-MR contrast agent. Doxorubicin hydrochloride (DOX), a well-known chemotherapeutic drug, was chosen as a model drug to assess the drug loading and releasing behaviors of the synthesized sample.

Experimental section

Materials

Tetraethyl orthosilicate (TEOS), 1,3,5-trimethylbenzene (TMB), and NH_4VO_3 were purchased from Sinopharm Chemical Reagent Co., Ltd.. *N*-Cetyltrimethylammonium bromide (CTAB) was obtained from Beijing Yili Chemical Co., Ltd. Gd_2O_3 and Eu_2O_3 (99.99%) were purchased from Science and Technology Parent Company of the Changchun Institute of Applied Chemistry. DOX was obtained from the Nanjing Duodian Chemical Limited Company. The other chemicals, including NaOH, concentrated HNO_3, HCl, citric acid, NaCl, polyethylene glycol, were all purchased from Beijing Chemical Regent Company. All the chemicals were analytical grade and used without further treatment.

Synthesis of MSN and $GdVO_4$:Eu^{3+}@MSN

Mesoporous silica nanoparticles were synthesized according to the literature with some modification.[25] 0.5 g of CTAB and 3.5 mL of TMB were successively added into a solution containing 250 mL of deionized water and 1.75 mL of 2 mol L^{-1} NaOH solution. After vigorous stirring at 80 °C for 4 h, 5.0 mL of TEOS was added into the mixture. Then, the reaction was vigorously stirred at 80 °C for another 2 h. The resultant white precipitate was separated by filtration, washed with ethanol and water, and dried overnight in a vacuum at 60 °C. The structure-template CTAB and TMB were removed by calcination at 650 °C for 6 h.

$GdVO_4$:Eu^{3+}@MSN was prepared by a Pechini sol–gel process. The doping concentration of Eu^{3+} was 5 mol% of Gd^{3+} in $GdVO_4$:Eu^{3+}, which had been optimized in our previous work.[53] Stoichiometric amounts of Gd_2O_3, Eu_2O_3 were dissolved in dilute HNO_3, under stirring, and the pH value of the solution was maintained between 2 and 3. Then a suitable amount of ammonium vanadium oxide (NH_4VO_3) was added to the solution. Citric acid (A. R.) was added to the above solution as a chelating agent for the metal ions. The molar ratio of metal ions to citric acid was 1 : 2. An appropriate amount of polyethylene glycol (PEG, M_w = 10 000) was added as a cross-linking agent. The mixture was stirred for 1 h to form a stable sol. Then the calcined MSNs were added into the sol with stirring. After further stirring for another 2 h, the resulting material was separated by centrifugation. The obtained sample was dried at 100 °C for 2 h and then heated from room temperature to 700 °C with a heating rate of 2 °C min^{-1} and maintained at this temperature for 2 h in air. Finally, the $GdVO_4$:Eu^{3+} functionalized MSN were obtained.

In vitro MRI assay

The MRI measurements were performed in a 0.5 T MRI magnet (Shanghai Niumai Corporation Ration NM120-Analyst). $GdVO_4$:Eu^{3+}@MSN samples were dispersed in water at various Gd concentrations. T_1 was acquired using an inversion recovery sequence. T_1 measurements were performed using a nonlinear fit to changes in the mean signal intensity within each well as a function of TR using the provided quantification software. Finally, the r_1 relaxivity value was determined through the curve fitting of $1/T_1$ relaxation time (s^{-1}) *vs.* the Gd concentration (mM).

Cell viability of $GdVO_4$:Eu^{3+}@MSN

The *in vitro* cytotoxicity of the $GdVO_4$:Eu^{3+}@MSN was determined by MTT (3-(4,5-dimethylthiazol-2-yl)-2,5-diphenyltetrazolium bromide) assays, and the Vero cell line was used here. L929 fibroblast cells (5000–6000) in 200 μL media per well were plated in a 96-well plate for 24 h to allow the cells to attach and then exposed to different concentrations of the samples (3.125, 6.25, 12.5, 25.0, 50.0, 100 and 200.0 μg mL^{-1}) for 24 h in 5% CO_2 at 37 °C. At the end of the incubation time, the medium containing the composite was removed and MTT solution (20 μL, diluted in a culture medium to a final concentration of 5 mg mL^{-1}) was added. After incubation at 37 °C in the dark for 4 h, 100 μL of acidified isopropanol was added to each well, and the absorbance was monitored with a microplate reader at a wavelength of 570 nm. Averages and standard deviations were based on four samples, and all tests were performed in triplicate. The cell viability was calculated using the following equation: cell viability (%) = [*A*]test/[*A*]control × 100.

Cell uptake

Cellular uptake by SKOV3 ovarian cancer cells was examined using flow cytometry. For flow cytometry studies, SKOV3 ovarian cancer cells (1×10^5) were seeded in 6-well culture plates and grown overnight. The cells were then treated with $GdVO_4$:Eu^{3+}@MSN-FITC or free FITC at 37 °C for 30 min, 3 h, 6 h, respectively. A single cell suspension was prepared consecutively by trypsinization, washing with PBS, and filtration through 35 mm nylon mesh. Thereafter, the cells were lifted using a cell stripper (Media Tech. Inc) and analyzed using a flow cytometer (FACS Calibur). Cells incubated in the absence of the composite were used as the control.

For CLSM, the A549 lung adenocarcinoma cells were seeded in 6-well culture plates (a lean cover slip was put in each well) and grown overnight as a monolayer, and were incubated with $GdVO_4$:Eu^{3+}@MSN-FITC at 37 °C for 30 min, 1 h, 6 h, respectively. Thereafter, the cells were rinsed with PBS three times, fixed with 2.5% formaldehyde (1 mL per well) at 37 °C for 10 min, and then rinsed with PBS three times again. For nucleus labeling, the nuclei were stained with Hoechst 33342 solution (from Molecular Probes, 20 mg mL^{-1} in PBS, 1 mL per well) for 10 min and then rinsed with PBS three times. The

cover slips were placed on a glass microscope slide, and the samples were visualized using CLSM (FV 10-ASW).

Drug loading and *in vitro* release

5 mg of $GdVO_4$:Eu^{3+}@MSN was dispersed in 0.5 mL deionized water, and 3.0 mL of DOX (1 mg mL^{-1}) was added into the above solution. The mixture was shaken for 24 h at room temperature in the dark to reach the equilibrium state. Then the solution was centrifuged to collect the DOX-loaded $GdVO_4$:Eu^{3+}@MSN sample. The supernatant solutions were collected, and the content of DOX was determined by UV-Vis spectroscopy at the wavelength of 480 nm. The drug loading content was calculated by the following equations: Loading content (%) = (weight of drug in particles/weight of drug loaded particles) × 100%. In the *in vitro* drug release experiment, DOX loaded $GdVO_4$:Eu^{3+}@MSN sample was immersed in 2 mL of PBS (pH = 7.4, 4.0, 2.0) at 37 °C. At selected time intervals, buffer solution was removed and replaced with fresh buffer solution. The amounts of released DOX in the supernatant were measured by UV-Vis spectrophotometry.

Characterization

The X-ray diffraction (XRD) measurements were performed on a D8 focus diffractometer (Bruker) with Cu-Kα radiation (λ = 0.15405 nm). The morphologies of the samples were obtained using a field emission scanning electron microscope (FE-SEM, S-4800, Hitachi). Transmission electron microscopy (TEM) was obtained using FEI Tecnai G2 S-Twin with a field emission gun operating at 200 kV. Images were acquired digitally on a Gatan multiple CCD camera. Inductively coupled plasma (ICP) measurements (Thermo iCAP 6000ICP-OES) were performed on the sample to determine the exact loading level of $GdVO_4$:Eu^{3+}. The X-ray photoelectron spectra (XPS) were taken on a VG ESCALAB MK II electron energy spectrometer using Mg Kα (1253.6 eV) as the X-ray excitation source. Nitrogen adsorption–desorption analysis was performed with a Micromeritics ASAP 2020 M apparatus. The specific surface area was determined by the Brunauer–Emmett–Teller (BET) method, and the pore size distributions were calculated by the Barrett–Joyner–Halenda (BJH) method. The UV-Vis adsorption spectral values were measured on a U-3310 spectrophotometer (Hitachi). The photoluminescence (PL) spectra were taken on an F-7000 spectrophotometer (Hitachi) equipped with a 150 W xenon lamp as the excitation source. Flow cytometry analysis was performed on a FACS Calibur flow cytometer (BD Biosciences) with 488 nm excitation lasers. CLSM images were observed with a confocal laser scanning microscope (Olympus, FV 1000). The ζ potential was measured using a Malvern Zetasizer Nano ZS 90.

Results and discussion

Fig. 1A displays the low-angle XRD patterns of the MSN and $GdVO_4$:Eu^{3+}@MSN. The samples exhibit three well-resolved diffraction peaks that can be indexed to (100), (110), (200) reflections associated with the hexagonal mesostructure

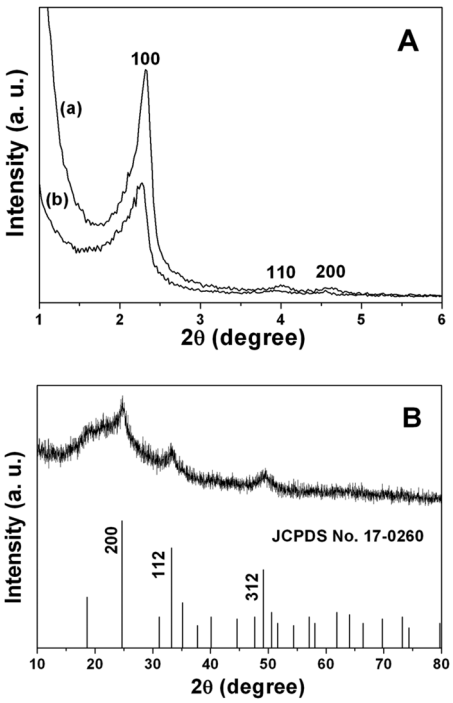

Fig. 1 A: Low-angle XRD patterns of (a) MSN, (b) $GdVO_4$:Eu^{3+}@MSN. B: Wide-angle XRD pattern of $GdVO_4$:Eu^{3+}@MSN.

(*p6mm*), confirming a well-ordered mesoporous structure in these materials. In addition, the results also indicate that the ordered mesoporous structure of MSN can be maintained after the deposition of $GdVO_4$:Eu^{3+} phosphor. However, the intensity of these characteristic diffractions decreases noticeably after the deposition of $GdVO_4$:Eu^{3+}, indicating that the integrity of the mesoporous structure (short range order) is decreased due to the deposition of $GdVO_4$:Eu^{3+} onto the mesoporous framework of MSN. Fig. 1B shows the wide-angle XRD pattern of the $GdVO_4$:Eu^{3+}@MSN, where the broad band at 2θ = 22° is the characteristic peak for amorphous SiO_2 (JCPDS 29-0085). The other diffraction peaks at 2θ = 24.67° (200), 33.23° (112), 49.15° (312) can be indexed to a pure tetragonal phase for $GdVO_4$ (JCPDS No. 17-0260), which suggests that $GdVO_4$:Eu^{3+} have crystallized well on the surfaces of the mesoporous silica nanoparticles. Additionally, no other phase related to the doped Eu^{3+} can be detected, revealing the successful substitution of Eu^{3+} for Gd^{3+} in the $GdVO_4$ host. The exact loading level of $GdVO_4$:Eu^{3+} on MSN was determined to be 16.82% by ICP measurement.

The SEM images of the samples are shown in Fig. 2(a, b), the calcined mesoporous silicas were revealed to be spherical particles with diameters in the range of 80–120 nm. After deposition of $GdVO_4$:Eu^{3+} nanoparticles, the morphology of the sample remains the same as the bare silica nanoparticles. A highly ordered mesoporous structure with a hexagonal array could be clearly seen in the TEM image of the pristine sample (Fig. 2c), which is characteristic of MCM-41 type MSN. The $GdVO_4$:Eu^{3+} nanoparticles can be seen as small black dots dispersed on the outside surface and in the pores of the MSN in

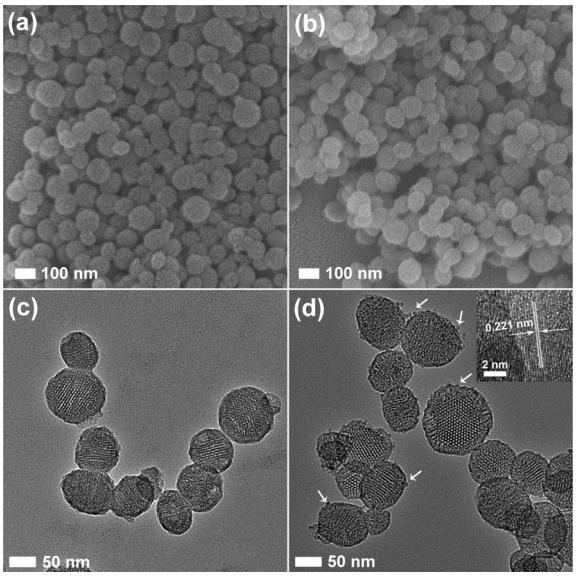

Fig. 2 SEM images of (a) MSN, (b) $GdVO_4$:Eu^{3+}@MSN. TEM images of (c) MSN, (d) $GdVO_4$:Eu^{3+}@MSN. Inset: HRTEM image of $GdVO_4$:Eu^{3+}.

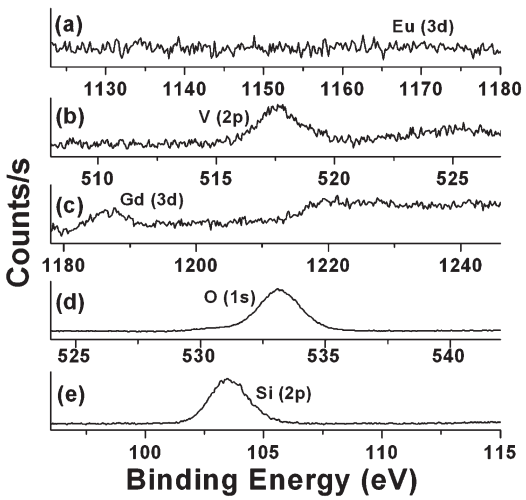

Fig. 3 XPS spectrum of $GdVO_4$:Eu^{3+}@MSN.

Fig. 2d (indicated by the arrows). As shown in the HRTEM image of $GdVO_4$:Eu^{3+}@MSN (inset image), the lattice fringes of the crystalline phase ($GdVO_4$:Eu^{3+}) can be clearly observed. The distance (0.221 nm) between the adjacent lattice fringes corresponds to the *d* (301) spacing (0.225 nm) of $GdVO_4$ (JCPDS No. 17-0260).

Fig. 3 presents the X-ray photoelectron spectra of the $GdVO_4$:Eu^{3+} loaded MSN. The binding energy peaks of Si (2p, 102.9 eV), O (1s, 531.9 eV), Gd (3d, 1188.7 eV), V (2p, 518.3 eV), and Eu (3d, 1170 eV) can be clearly seen in Fig. 3. By combination of previous XRD results, it can be deduced that these signals arise from $GdVO_4$:Eu^{3+} (a–d) and MSN (d, e). XPS results provide additional evidence for the deposition of crystalline $GdVO_4$:Eu^{3+} on the surface of MSN.

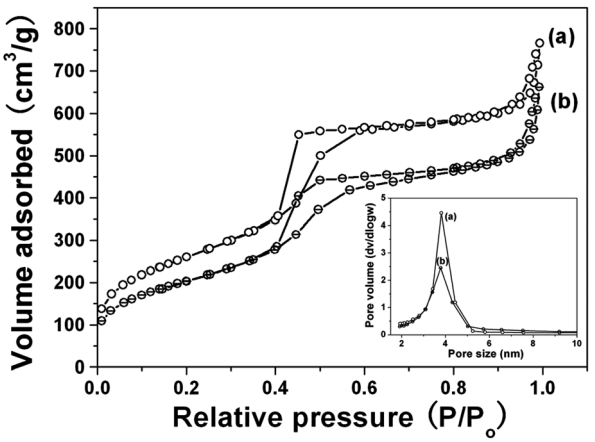

Fig. 4 N_2 adsorption/desorption curves and pore size distribution curves (inset) of the samples. (a) MSN, (b) $GdVO_4$:Eu^{3+}@MSN.

In order to obtain the MSN with pore sizes large enough to accommodate drug molecules, TMB was added during the synthetic process. According to the N_2 sorption results (Fig. 4), the MSN have high specific area (587 m^2 g^{-1}) and large pore volume (0.780 cm^3 g^{-1}). The average pore size of the MSN was 4.27 nm. After the deposition of $GdVO_4$:Eu^{3+} nanoparticles, the BET surface area and pore volume of $GdVO_4$:Eu^{3+}@MSN decreased to 462 m^2 g^{-1} and 0.671 cm^3 g^{-1}, respectively. The average pore size decreased to 4.15 nm. This is because some of the pore entrances were blocked by the $GdVO_4$:Eu^{3+} nanoparticles.

Fig. 5 shows the excitation and emission spectra of $GdVO_4$:Eu^{3+}@MSN. The excitation spectrum was obtained by monitoring the emission of the Eu^{3+} $^5D_0$–$^7F_2$ transition at 620 nm. It can be seen clearly that the excitation spectrum consists of a strong and broad band with a maximum at about 280 nm and a shoulder around 250 nm. The former can be attributed to the $GdVO_4$ host (VO_4^{3-}) excitation band, and the latter is due to the ^8S–^6D (250 nm) transition of Gd^{3+}.[54] The general f–f transition lines of Eu^{3+} in the longer wavelength region have not been observed due to their relatively weak intensity compared with the strong $GdVO_4$ host excitation band. The presence of the strong $GdVO_4$ host band in the excitation spectrum of Eu^{3+} indicates that there exists an efficient energy transfer from the $GdVO_4$ host to the doped Eu^{3+}. Excitation into the $GdVO_4$ host band at 280 nm yields the emission spectrum corresponding to f–f transitions of Eu^{3+}, which is dominated by the hypersensitive red emission $^5D_0$–$^7F_2$ transition at 620 nm. The location of the emission lines of Eu^{3+} and their assignments are indicated in Fig. 5B. Obviously, the strong emission of Eu^{3+} is due to an efficient energy transfer from the VO_4^{3-} group to Eu^{3+} in $GdVO_4$:Eu^{3+}@MSN. The $^5D_0$–$^7F_2$ emission of Eu^{3+} arises from a hypersensitive transition with $\Delta J = 2$, which is strongly influenced by the surroundings. When the Eu^{3+} is located at a low-symmetry local site (without an inversion center), this emission transition often dominates in the emission spectrum. This is actually the case for Eu^{3+} in the $GdVO_4$ host lattices. The luminescent intensity of

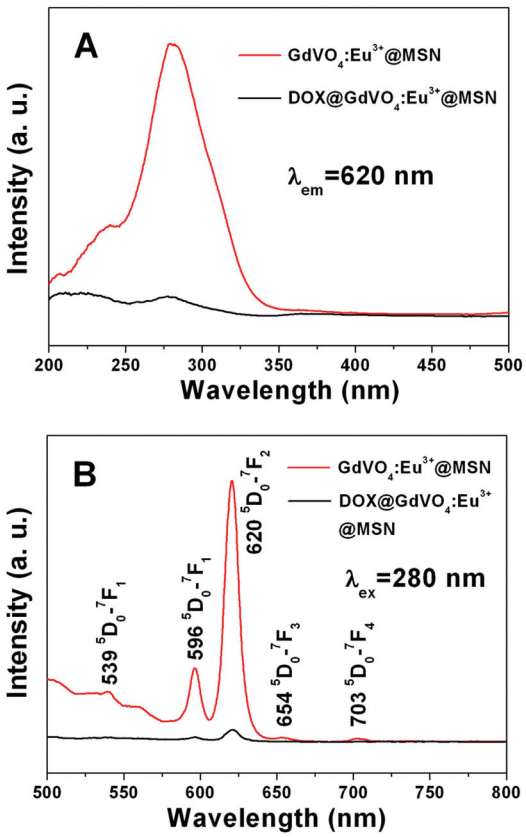

Fig. 5 Excitation (A) and emission (B) spectra of $GdVO_4$:Eu^{3+}@MSN, DOX@$GdVO_4$:Eu^{3+}@MSN.

DOX-$GdVO_4$:Eu^{3+}@MSN decreased drastically, which may be related to the loading of DOX molecules that quench the emission of Eu^{3+}. However, the luminescence can still be detected during the drug release process, suggesting its potential application in the biomedical field.

To evaluate the potential application of $GdVO_4$:Eu^{3+}@MSN as MR imaging contrast agents, the T_1 relaxation time was measured in aqueous dispersions with different Gd^{3+} concentrations. As shown in Fig. 6a, the longitudinal relaxivity (r_1) was estimated to be 0.57 s^{-1} mM^{-1} from the slope of the relaxation rate ($1/T_1$) as a function of Gd^{3+} concentration. In a proof-of-concept application as MR imaging contrast agents, representative T_1-weighted MR images of the $GdVO_4$:Eu^{3+}@MSN suspensions clearly showed positive signal enhancement of the effect on T_1-weighted sequences as the Gd^{3+} concentration increased, resulting in brighter images (Fig. 6b). These results suggest that the $GdVO_4$:Eu^{3+}@MSN can be potentially employed as an effective T_1 contrast agent.

The stability and cytotoxicity are important considerations for the actual application as a potential drug carrier in biomedical fields. To evaluate the biocompatibility of $GdVO_4$:Eu^{3+}@MSN, the standard MTT cell assay was used on the L929 fibroblast cells. As shown in Fig. 7, the samples do not show apparent cytotoxicity against the L929 fibroblast cells after incubation for 24 h. The concentration of the composite was as high as 200 μg mL^{-1}, at which the cell viability remained at

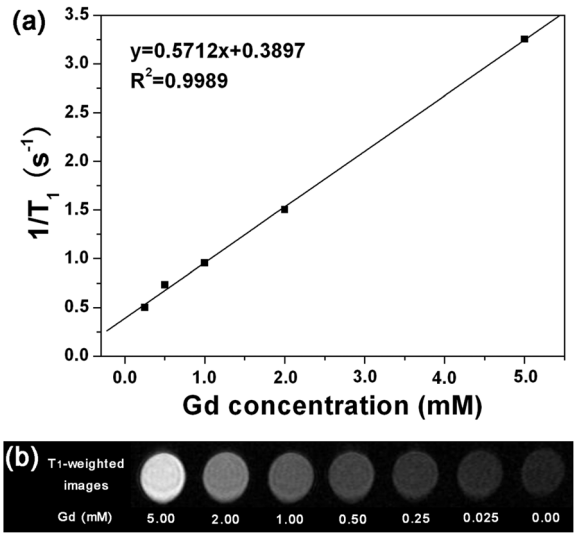

Fig. 6 (a) Relaxation rate r_1 ($1/T_1$) *versus* various molar concentrations of $GdVO_4$:Eu^{3+}@MSN dispersions at room temperature using 0.5 T MRI magnet. (b) T_1 weighted images of various molar concentrations of Gd^{3+} in $GdVO_4$:Eu^{3+}@MSN.

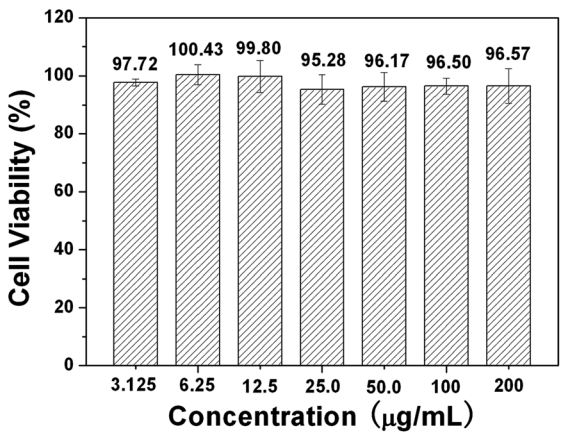

Fig. 7 Relative cell viabilities of L929 cells incubated with different concentrations of $GdVO_4$:Eu^{3+}@MSN.

96.57%. The results indicate that the composite has good biocompatibility and can be potentially used as drug carriers in biomedical applications.

The $GdVO_4$:Eu^{3+}@MSN was labeled with fluorescent dye, fluorescein isothiocyanate (FITC), so the cell uptake degree of the composites could be quantified with flow cytometry by determining the green fluorescence emitted from $GdVO_4$:Eu^{3+}@MSN-FITC treated SKOV3 cells. As can be seen in Fig. 8, after incubation of SKOV3 cells with the sample for different time periods (30 min, 3 h, 6 h), the cell-labeling ability of $GdVO_4$:Eu^{3+}@MSN-FITC composites was estimated by flow cytometry. $GdVO_4$:Eu^{3+}@MSN-FITC composites were taken up by SKOV3 cells compared to the controlled cells, and the cell uptake of sample increases with incubation time.

To further verify the location of the particles relative to the cells, the confocal laser scanning microscopy (CLSM)

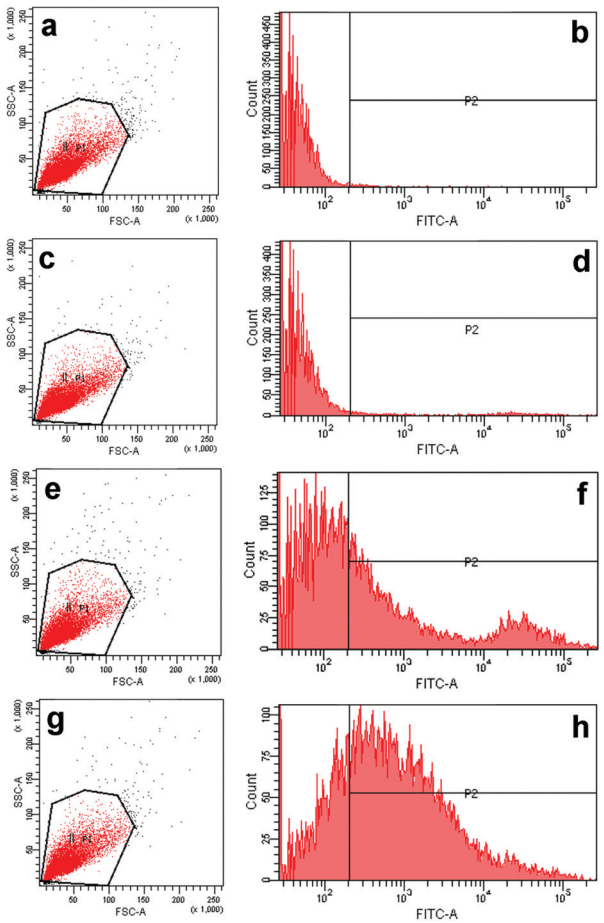

Fig. 8 Flow cytometry analysis of the control cells (a, b) and SKOV3 cells incubated with $GdVO_4:Eu^{3+}$@MSN-FITC composites for 30 min (c, d), 3 h (e, f), 6 h (g, h).

photographs of A549 lung adenocarcinoma cells incubated with FITC labeled $GdVO_4:Eu^{3+}$@MSN for 30 min, 1 h, and 6 h at 37 °C are shown in Fig. 9. The green fluorescence of FITC can be clearly seen in the confocal images with an excitation wavelength of 488 nm. In the first 30 min, the green FITC appears localized as scattered dots, which demonstrate that only a few of the nanoparticles were taken up by A549 lung adenocarcinoma cells. With the increase of the incubation time, the intensities of the green signal increase, that is, more particles have crossed the membrane and localized in the cytoplasm. The results confirm that as-prepared samples can be effectively taken up by A549 lung adenocarcinoma cells.

The loading level of DOX in $GdVO_4:Eu^{3+}$@MSN is calculated to be 14%. DOX is known for its ability to strongly attach to the silica surface, due to formation of strong hydrogen bonds and charge interaction with surface silanols. Because of the weak-acid property of the silanols (–Si–OH), silica presents a negatively charged surface (–Si–O–) in neutral or basic surroundings, which has a strong interaction with the positively charged DOX molecules due to the protonated primary amine group on DOX. The *in vitro* drug release behavior of DOX@$GdVO_4:Eu^{3+}$@MSN was studied in solutions with

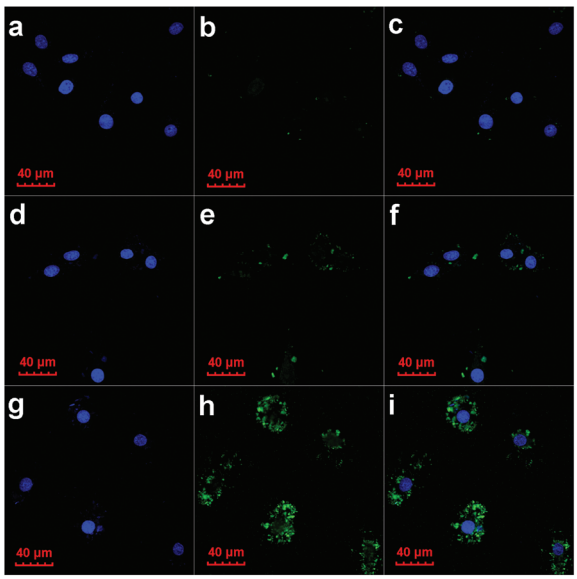

Fig. 9 CLSM images of A549 cells incubated with $GdVO_4:Eu^{3+}$@MSN-FITC composites for 30 min (a–c), 1 h (d–f), and 6 h (g–i) at 37 °C. Each column can be classified as the nuclei of cells (being dyed blue by Hoechst 33342 for visualization), $GdVO_4:Eu^{3+}$@MSN-FITC, and a merge of the two channels, respectively.

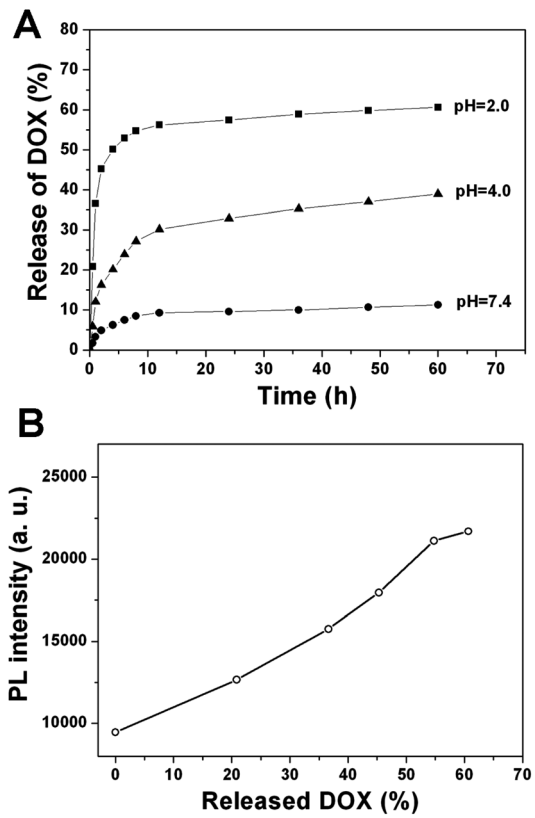

Fig. 10 (A) Release of DOX in media with different pH values. (B) PL emission intensity of Eu^{3+} in $GdVO_4:Eu^{3+}$@MSN as a function of the cumulatively released DOX in PBS (pH = 2.0).

different pH values. As can be seen in Fig. 10A, the DOX release rate is faster at acidic pH than at neutral pH 7.4.

The cumulative release of DOX could reach 61% after 60 h at pH 2.0, much higher than that at pHs 4.0 and 7.4, which was 39% and 11%. The ζ potential values of the sample were −2.6, −10.2, −20.3 mV in pH 2.0, 4.0, 7.4 PBS buffer, respectively. It can be seen that the sample shows a more negative ζ potential with increasing pH, which would result in stronger interaction with the positively charged DOX molecules. The release rate of DOX *in vitro* increased with decreasing pH values. Lower pH leads to the increased hydrophilicity and higher solubility of DOX by increasing protonated $-NH_2$ groups on DOX, which cause repulsion between silica and DOX. The pH-sensitive DOX release can occur across the range of pH values found in intracellular lysosomes (pH ~ 4), or in the unique strongly acid environment in the stomach (pH 1.5–3.5), thereby enabling targeted therapeutic capacity by passive release at the pathologically relevant sites.[16,38,55–58] These results show that the composite may find potential for pH controlled release in the acidic environment of tumor areas (such as gastric cancer) rather than at the physiologically neutral pH of normal tissue or biological fluids.

The emission intensity of $GdVO_4$:Eu^{3+}@MSN was greatly quenched after loading DOX and was recovered with the continued release of DOX. As shown in Fig. 10B, the PL intensity increases with the cumulative release time of DOX in PBS at pH 2.0. It is well known that the emission of rare earth ions can be quenched to some extent in environments with high phonon frequency.[54] The organic groups in DOX molecules with high-frequency vibrations will quench the emission of Eu^{3+} to a great extent. Upon the release of DOX, the quenching effect was weakened, leading to the increase of emission intensity. Additionally, the large amount of DOX molecules loaded onto the $GdVO_4$:Eu^{3+}@MSN will block the emission of the Eu^{3+} and the blocking effect may be attenuated with the release of DOX. The emission intensity of $GdVO_4$:Eu^{3+} was correlated with the loading and cumulative release of DOX molecules, which has potential to be used as a luminescence tag for identification, tracking and monitoring the release of the drug during biological research or disease therapy.

Conclusions

Mesoporous silica nanoparticles with diameters in the range of 80–120 nm were functionalized with luminescent $GdVO_4$:Eu^{3+} phosphor *via* a Pechini sol–gel method. The sample could be a candidate for a T_1-MR contrast agent due to the existence of Gd^{3+} ions in the composite. MTT measurements demonstrated that these nanoparticles had low cytotoxicity. Flow cytometry was used to confirm the internalization of the composite by SKOV3 ovarian cancer cells. CLSM results demonstrate that the samples can be effectively taken up by A549 lung adenocarcinoma cells. The drug release rate of DOX@$GdVO_4$:Eu^{3+}@MSN was pH dependent and increased with decreasing pH. The emission intensity of Eu^{3+} in $GdVO_4$:Eu^{3+}@MSN was correlated with the loading and cumulative release of DOX molecules, which shows potential for use in luminescent tagging. The composite can potentially act as a multifunctional drug carrier system with luminescent tagging, MR imaging and pH-controlled release property for DOX.

Acknowledgements

This project is financially supported by National Basic Research Program of China (2010CB327704), the National Natural Science Foundation of China (NSFC 51172228, 51272248, 21101149, 21221061).

Notes and references

1 G. Ferey, C. Mellot-Draznieks, C. Serre, F. Millange, J. Dutour, S. Surble and I. Margiolaki, *Science*, 2005, **309**, 2040.
2 T. Azaus, C. Tournq-Pqteilh, F. Aussenac, N. Baccile, C. oelho, J. M. Devoisselle and F. Babonneau, *Chem. Mater.*, 2006, **18**, 6382.
3 J. Fan, C. Yu, F. Gao, J. Lei, B. Tian, L. Wang, Q. Luo, B. Tu, W. Zhou and D. Zhao, *Angew. Chem., Int. Ed.*, 2003, **42**, 3146.
4 M. Vallet-Regi, A. Rámila, R. P. el Real and J. Pérez-Pariente, *Chem. Mater.*, 2001, **13**, 308.
5 M. Vallet-Regi, F. Balas and D. Arcos, *Angew. Chem., Int. Ed.*, 2007, **46**, 7548.
6 I. I. Slowing, B. G. Trewyn, S. Giri and V. S. Y. Lin, *Adv. Funct. Mater.*, 2007, **17**, 1225.
7 F. Y. Qu, G. S. Zhu, S. Y. Huang, S. G. Li, J. Y. Sun, D. L. Zhang and S. L. Qiu, *Microporous Mesoporous Mater.*, 2006, **92**, 1.
8 J. Andersson, J. Rosenholm, S. Areva and M. Linden, *Chem. Mater.*, 2004, **16**, 4160.
9 N. K. Mal, M. Fujiwara, Y. Tanaka, T. Taguchi and M. Matsukata, *Chem. Mater.*, 2003, **15**, 3385.
10 T. D. Nguyen, K. C.-F. Leung, M. Liong, Y. Liu, J. F. Stoddart and J. I. Zink, *Adv. Funct. Mater.*, 2007, **17**, 2101.
11 C. Park, K. Lee and C. Kim, *Angew. Chem., Int. Ed.*, 2009, **48**, 1275.
12 C. Y. Lai, B. G. Trewyn, D. M. Jeftinija, K. Jeftinija, S. Xu, S. Jeftinija and V. S.-Y. Lin, *J. Am. Chem. Soc.*, 2003, **125**, 4451.
13 A. Schlossbauer, J. Kecht and T. Bein, *Angew. Chem., Int. Ed.*, 2009, **48**, 3092.
14 B. G. Trewyn, S. Giri, I. I. Slowing and V. S.-Y. Lin, *Chem. Commun.*, 2007, 3236.
15 K. M. L. Taylor, J. S. Kim, W. J. Rieter, H. An and W. Lin, *J. Am. Chem. Soc.*, 2008, **130**, 2154.
16 B. G. Trewyn, N. Z. Knežević and V. S. Y. Lin, *Chem.–Eur. J.*, 2011, **17**, 3339.
17 C. Lei, Y. Shin, J. Liu and E. J. Ackerman, *J. Am. Chem. Soc.*, 2002, **124**, 11242.
18 H. Zheng, Y. Wang and S. Che, *J. Phys. Chem. C*, 2011, **115**, 16803.

19 L. E. Gerweck, *Semin. Radiat. Oncol.*, 1998, **8**, 176.
20 J. L. Wike-Hooley, J. Haveman and H. S. Reinhold, *Radiother. Oncol.*, 1984, **2**, 343.
21 S. H. Cheng, W. N. Liao, L. M. Chen and C.-H. Lee, *J. Mater. Chem.*, 2011, **21**, 7130.
22 R. Casasús, M. D. Marcos, R. Martínez-Máñez, J. V. Ros-Lis, J. Soto, L. A. Villaescusa, P. Amorós, D. Beltrán, C. Guillem and J. Latorre, *J. Am. Chem. Soc.*, 2004, **126**, 8612.
23 R. Casasús, E. Climent, M. D. Marcos, R. Martínez-Máñez, F. Sancenón, J. Soto, P. Amorós, J. Cano and E. Ruiz, *J. Am. Chem. Soc.*, 2008, **130**, 1903.
24 R. Liu, P. H. Liao, J. K. Liu and P. Y. Feng, *Langmuir*, 2011, **27**, 3095.
25 L. Yuan, Q. Q. Tang, D. Yang, J. Z. Zhang, F. Y. Zhang and J. H. Hu, *J. Phys. Chem. C*, 2011, **115**, 9926.
26 Y. Zhu, J. Shi, W. Shen, X. Dong, J. Feng, M. Ruan and Y. Li, *Angew. Chem., Int. Ed.*, 2005, **44**, 5083.
27 Q. Yang, S. Wang, P. Fan, L. Wang, Y. Di, K. Lin and F. S. Xiao, *Chem. Mater.*, 2005, **17**, 5999.
28 S. W. Song, K. Hidajat and S. Kawi, *Chem. Commun.*, 2007, 4396.
29 W. Xu, Q. Gao, Y. Xu, D. Wu and Y. Sun, *Mater. Res. Bull.*, 2009, **44**, 606.
30 A. Popat, J. Liu, G. Q. (Max) Lua and S. Z. Qiao, *J. Mater. Chem.*, 2012, **22**, 11173.
31 T. D. Nguyen, K. C. F. Leung, M. Liong, C. D. Pentecost, J. F. Stoddart and J. I. Zink, *Org. Lett.*, 2006, **8**, 3363.
32 K. C. F. Leung, T. D. Nguyen, J. F. Stoddart and J. I. Zink, *Chem. Mater.*, 2006, **18**, 5919.
33 C. Park, K. Oh, S. C. Lee and C. Kim, *Angew. Chem., Int. Ed.*, 2007, **46**, 1455.
34 Y. L. Zhao, Z. X. Li, S. Kabehie, Y. Y. Botros, J. F. Stoddart and J. I. Zink, *J. Am. Chem. Soc.*, 2010, **37**, 13016.
35 F. Muhammad, M. Y. Guo, W. X. Qi, F. X. Sun, A. F. Wang, Y. J. Guo and G. Zhu, *J. Am. Chem. Soc.*, 2011, **133**, 8778.
36 R. Liu, Y. Zhang, X. Zhao, A. Agarwal, L. J. Mueller and P. Y. Feng, *J. Am. Chem. Soc.*, 2010, **132**, 1500.
37 Y. H. Ma, L. Zhou, H. Q. Zheng, L. Xing, C. G. Li, J. H. Cui and S. A. Che, *J. Mater. Chem.*, 2011, **21**, 16869.
38 Z. Y. Cheng, P. A. Ma, Z. Y. Hou, W. X. Wang, Y. L. Dai, X. F. Zhai and J. Lin, *Dalton Trans.*, 2012, **41**, 1481.
39 B. Wang, C. Xu, J. Xie, Z. Yang and S. Sun, *J. Am. Chem. Soc.*, 2008, **130**, 14436.
40 B. G. Trewyn, J. A. Nieweg, Y. Zhao and V. S. Y. Lin, *Chem. Eng. J.*, 2008, **137**, 23.
41 C. Lei, Y. Shin, J. Liu and E. J. Ackerman, *J. Am. Chem. Soc.*, 2002, **124**, 11242.
42 H. Q. Zheng, Z. H. Huang and S. A. Che, *Dalton Trans.*, 2012, **41**, 5038.
43 Y. Zheng, H. You, G. Jia, K. Liu, Y. Song, M. Yang and H. Zhang, *Cryst. Growth Des.*, 2009, **9**, 5101.
44 I.-F. Li, C.-H. Su, H.-S. Sheu, H.-C. Chiu, Y.-W. Lo, W.-T. Lin, J.-H. Chen and C.-S. Yeh, *Adv. Funct. Mater.*, 2008, **18**, 766.
45 J. Zhou, M. X. Yu, Y. Sun, X. Z. Zhang, X. J. Zhu, Z. H. Wu, D. M. Wu and F. Y. Li, *Biomaterials*, 2011, **32**, 1148.
46 J. Zhou, Y. Sun, X. X. Du, L. Q. Xiong, H. Hu and F. Y. Li, *Biomaterials*, 2010, **31**, 3287.
47 Q. Ju, Y. S. Liu, D. T. Tu, H. M. Zhu, R. F. Li and X. Y. Chen, *Chem.–Eur. J.*, 2011, **17**, 8549.
48 G. Tian, Z. J. Gu, X. X. Liu, L. J. Zhou, W. Y. Yin, L. Yan, S. Jin, W. L. Ren, G. M. Xing, S. J. Li and Y. L. Zhao, *J. Phys. Chem. C*, 2011, **115**, 23790.
49 B. K. Gupta, V. Rathee, T. N. Narayanan, P. Thanikaivelan, A. Saha, Govind, S. P. Singh, V. Shanker, A. A. Marti and P. M. Ajaya, *Small*, 2011, **13**, 1767.
50 S. Li, H. liu, L. Li, N. Q. Luo, R. H. Cao, D. H. Chen and Y. Z. Shao, *Appl. Phys. Lett.*, 2011, **98**, 093704.
51 X. J. Kang, Z. Y. Cheng, D. M. Yang, P. A. Ma, M. M. Shang, C. Peng, Y. L. Dai and J. Lin, *Adv. Funct. Mater.*, 2012, **22**, 1470.
52 X. J. Kang, D. M. Yang, Y. L. Dai, M. M. Shang, Z. Y. Cheng, X. Zhang, H. Z. Lian, P. A. Ma and J. Lin, *Nanoscale*, 2013, **5**, 253.
53 G. Z. Li, Z. L. Wang, M. Yu, Z. W. Quan and J. Lin, *J. Solid State Chem.*, 2006, **179**, 2698.
54 G. Blasse and B. C. Grabmeter, *Luminescent Materials*, Springer, Berlin, 1994.
55 L. L. Li, F. Q. Tang, H. Y. Liu, T. L. Liu, N. J. Hao, D. Chen, X. Teng and J. Q. He, *ACS Nano*, 2010, **4**, 6874.
56 G. Helmlinger, F. Yuan, M. Dellian and R. K. Jain, *Nat. Med.*, 1997, **3**, 177.
57 Y. F. Zhu, T. Ikoma, N. Hanagata and S. Kaskel, *Small*, 2010, **6**, 471.
58 F. Zhang, G. B. Braun, A. Pallaoro, Y. C. Zhang, Y. F. Shi, D. X. Cui, M. Moskovits, D. Y. Zhao and G. D. Stucky, *Nano Lett.*, 2012, **12**, 61.